Product Energy and Angular Momentum Partitioning in the Unimolecular Dissociation Of Aluminum Clusters†

Gilles H. Peslherbe*

Department of Chemistry and Biochemistry, 1455 De Maisonneuve Blvd. West, Concordia University, Montréal, Québec H3G 1M8, Canada

William L. Hase

Department of Chemistry, Wayne State University, Detroit, Michigan 48202-3489

Received: March 30, 2000

A previous classical trajectory simulation showed that the unimolecular decompositions of Al_6 and Al_{13} are intrinsically RRKM. In the work presented here, this study is further analyzed to determine the $Al_5 + Al$ and $Al_{12} + Al$ product energy distributions, which are compared with the predictions of statistical theories. Orbiting transition state/phase space theory (OTS/PST) gives distributions in excellent agreement with the trajectory results. Assuming a loose, product-like transition state gives a lower average product translational energy, $\langle E_t \rangle$, than what is found with the orbiting transition state. Including anharmonicity, in the calculation of the product vibrational density of states, increases the energy partitioned to product vibration. The Engelking model for cluster decomposition overestimates $\langle E_t \rangle$. One Klots model gives an inaccurate $\langle E_t \rangle$, but a second model more firmly rooted in phase space theory performs quite well. The Engelking model, for deducing the cluster dissociation energy from the measured $\langle E_t \rangle$, does not give accurate results for Al_6 and Al_{13} dissociation.

I. Introduction

Clusters allow one to study how physical and chemical properties change in the transition from an isolated molecule to a condensed phase environment.[1,2] The changes in a variety of structural, energetic, and kinetic properties during this transition are of interest. With clusters one can study the effect of microsolvation on chemical reactivity, model surface processes on a microscopic scale, and study how the transition from molecular to condensed-phase properties depends on system size.

Properties of small clusters such as equilibrium structures, binding energies, and electronic energy levels may now be studied in more detail with recent advances in electronic structure theory. Meanwhile, experimental studies of cluster unimolecular decay are legion, focusing on fragmentation rates, product size distributions, and product energy partitioning.[3−10] One of the main goals of these experiments is to determine cluster binding energies, which in turn can be compared to the predictions of electronic structure theory. However, the parent cluster internal energies are not known in the experiments, and one often uses statistical models to predict the possible internal energy distributions of the cluster prior to dissociation. Statistical models in general play a key role in the determination of binding energies from experimental observables.[11]

Cluster binding energies may be deduced from experimental measurements by statistical analysis of (1) energy-resolved collision-induced dissociation cross sections; (2) photodissociation lifetimes; and (3) product energy distributions. In the first approach, the collision-induced dissociation cross section is fit, as a function of relative collision energy, to an empirical law. Because the time scale for cluster dissociation can exceed the finite experimental time window for increasingly larger and complex clusters, the usual energy-dependent expression for the collision-induced dissociation cross section has been corrected for the finite cluster lifetime.[12−14] Statistical theories such as phase space theory or Rice-Ramsperger-Kassel-Marcus (RRKM) theory[11] are then used to estimate the cluster lifetimes. Similarly, one can fit experimentally measured cluster photodissociation lifetimes to a statistical rate theory expression and extract the cluster binding energy as the activation energy for dissociation, i.e., the energy of the transition state.[15,16] Both experimental methods were applied to Al_n^+ and Cu_n^+ clusters,[17,18] and the resulting cluster binding energies estimated with both approaches are systematically off by a few electronvolts. It is not clear at this point which approach is in error and whether the discrepancy arises from the particular choice of statistical model and parameters, but the binding energies determined from the energy-resolved collision-induced dissociation cross sections seem to be in better agreement with the predictions of the latest ab initio calculations.[19]

A third approach to "measure" cluster binding energies consists of analyzing the product translational energy, for the dissociation of metastable cluster ions, with statistical models proposed by Engelking[5,6] and Klots.[20−22] The Engelking model allows one to extract the binding energies with one adjustable parameter from the experimental average translational energy. This model has been applied to $(CO_2)_n^+$ clusters[6] and $\{(NH_3)_n$-$CH_3CN\}H^+$ and $(NH_3)_nH^+$ clusters.[23] In the latter application,[23] remarkable agreement was observed with the literature values of the cluster binding energies determined from equilibrium studies. However, Engelking translational energy distributions were found to be only approximate, when compared to the results of molecular dynamics simulations and accurate phase space theory calculations.[24] The other statistical family of models

† Part of the special issue "C. Bradley Moore Festschrift".

10.1021/jp0012146 CCC: $19.00
Published on Web 10/25/2000

used to extract structural information from the experimental translational energy for metastable cluster dissociation is based on the Klots theory of cluster evaporation.[20−22] This model was applied with some success to a number of clusters, including $(H_2O)_nH^+$ clusters[10] and $\{(NH_3)_nCH_3CN\}H^+$ and $(NH_3)_nH^+$ clusters.[23,25] The advantage of the Klots evaporative ensemble approach over the Engelking model is that both cluster heat capacities and binding energies can be determined with no adjustable parameter. Klots theory has been used for a wide variety of applications, such as the (statistical) modeling of the competitive coordination of different solvent molecules in mixed ligand−metal complexes,[26] and to estimate cluster temperatures or internal energies.[27]

In previous work, classical trajectory simulations were used to study the unimolecular dissociations dynamics of the aluminum clusters Al_n, $n = 3,6,13$.[28−30] Rapid intramolecular vibrational energy redistribution was observed for these clusters, and when excited randomly at fixed energy and angular momentum, they dissociated with a time-independent unimolecular rate constant indicating intrinsic RRKM behavior.[31] However, because of their highly fluxional character, resulting in extensive anharmonicity,[28−30] accurate anharmonic values for the transition state sum of states $N\ddagger(E)$ and density of states $\rho(E)$ are required to determine the RRKM rate constant from the expression

$$k(E) = \frac{N^{\ddagger}(E)}{h\rho(E)} \tag{1}$$

These anharmonic $N\ddagger(E)$ and $\rho(E)$ were determined numerically, from the potential energy surface used in the trajectory simulations.[28,30]

The present paper addresses the nature of the product energy and angular momentum distributions for dissociation of the Al_6 and Al_{13} clusters. The distributions obtained from the trajectory simulations are compared with the predictions of phase space theory[32−38] and the Engelking[5,6] and Klots[20−22] statistical models. It is of interest to test various statistical models for predicting product energy and angular momentum partitioning in cluster dissociation. Such an analysis of the Engelking and Klots models is particularly relevant, since they are widely used to extract binding energies from experimental translational energies but are based on a number of approximations. A preliminary and very incomplete report of this study has been given previously.[39]

II. Trajectory Simulations

The trajectory simulations reported here, of Al_6 and Al_{13} dissociation, were performed with the general chemical dynamics computer program VENUS.[40] The potential energy function and methodology used for the simulations are the same as those used previously.[30] The potential function is a model derived from ab initio calculations[41] and is written as a sum of two-body Lennard-Jones (L-J) potentials

$$V_{ij} = \epsilon\left[\left(\frac{r_0}{r_{ij}}\right)^{12} - 2\left(\frac{r_0}{r_{ij}}\right)^{6}\right] \tag{2}$$

and three-body Axilrod-Teller (A-T) potential functions

$$V_{ijk} = Z\epsilon {r_0}^9 \frac{1 + 3\cos\alpha_i \cos\alpha_j \cos\alpha_k}{(r_{ij}r_{jk}r_{ki})^3} \tag{3}$$

where $\epsilon = 26.52$ kcal/mol, $r_0 = 2.635$ Å, and $Z = 0.5$.

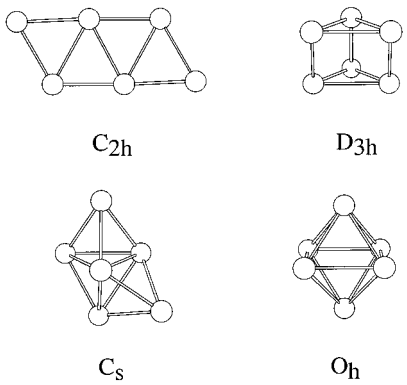

Figure 1. Some of the lowest potential energy minima for the Al_6 cluster on the L-J/A-T potential energy surface; eqs 2 and 3.

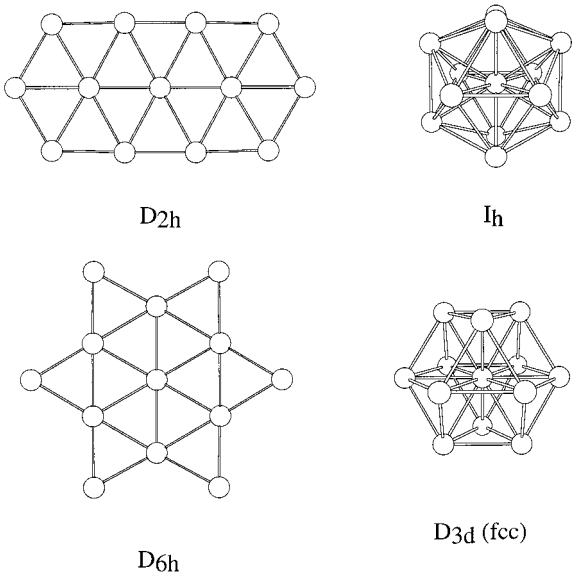

Figure 2. Same as Figure 1, but for the Al_{13} cluster.

Some of the lowest energy potential energy minima, given by this L-J/A-T potential for Al_6 and Al_{13} are shown in Figures 1 and 2. For Al_6, the C_{2h} structure has the lowest energy with a classical $Al_6 \rightarrow Al_5 + Al$ dissociation energy of 43.8 kcal/mol. The dissociation energy for the D_{3h}, C_s, and O_h structures are 40.0, 39.6, and 38.8 kcal/mol, respectively. For the Al_{13} cluster, the D_{2h} structure has the lowest energy with a classical $Al_{13} \rightarrow Al_{12} + Al$ dissociation energy of 56.2 kcal/mol. The D_{6h}, D_{3d}, and I_h structures have dissociation energies of 41.0, 15.5, and 2.2 kcal/mol, respectively. The products Al_5 and Al_{12} both have a minimum energy structure with C_{2v} symmetry.

Aluminum cluster geometries, predicted by the latest ab initio calculations, undergo a transition from a two-dimensional to a three-dimensional structure at cluster size of six or so.[19] This is attributed to a change in the cluster electronic structure; i.e., aluminum essentially behaves as a monovalent atom in small clusters while it behaves as a trivalent atom in the larger clusters.[17] The cluster minimum energy structures on the L-J/A-T potential energy surface are in good agreement with the predictions of ab initio calculations, especially for the smaller clusters.[19,41] However, the L-J/A-T model introduces too much planarity in the cluster structures; i.e., the L-J/A-T minimum structure for Al_{13} is planar while the ab initio calculations predict a more compact three-dimensional geometry. Finally, the energetics of cluster dissociation are very well reproduced by the L-J/A-T model. The dissociation energies of Al_6 and Al_{13} are 43.8 and 56.2 kcal/mol on the L-J/A-T potential energy

surface, respectively, while the latest ab initio calculations predict values of 44.2 and 61.2 kcal/mol.[19] Other analytic potential energy functions for Al_n clusters[42−46] were derived with the goal of reproducing bulk properties and do not describe small clusters as well as does the L-J/A-T potential.

Microcanonical normal mode sampling[47,48] was used to prepare initial microcanonical ensembles about the C_{2h}, C_{2v}, and O_h minima of the Al_6 cluster and about the D_{2h} and D_{3d} (fcc) minima of the Al_{13} cluster. Classical trajectories were used to study the dissociation of each of these ensembles. The dissociation of each ensemble is intrinsically RRKM, as described in the Introduction. In addition, the rate constants and product energy and angular momentum partitioning for Al_6 and Al_{13} are independent of the specific potential energy minima sampled in the initial conditions and only depend on the total energy (E) and angular momentum (J). Apparently, the intramolecular dynamics of the Al_6 and Al_{13} clusters is sufficiently chaotic that a microcanonical ensemble is quickly prepared over the complete phase space of the clusters.

Since sampling about different minima of Al_6 and Al_{13}, at fixed energy E and J, give the same results within statistical uncertainties, the product energy and angular momentum distributions calculated for the initial ensembles about the different minima of a cluster were combined to form the distributions reported here. The distributions considered here for $Al_n \rightarrow Al_{n-1} + Al$ dissociation are those for $Al_{n-1} + Al$ relative translational energy, E_t; Al_{n-1} internal (vibrational−rotational) energy, E_{int}; Al_{n-1} vibrational energy, E_v; and Al_{n-1} angular momentum, j.

III. Statistical Theories

A. Phase Space Theory. *1. Fundamentals.* Phase space theories[32−38] have been widely used to calculate product energy and angular momentum distributions for chemical reactions. In the early development of phase space theory, a loose transition state is assumed with properties identical to those of the reaction products. The loose transition state limit of phase space theory, identified here as PST, assumes that the reaction potential energy surface is of no importance for predicting the product properties. Other versions of phase space theory, identified here as orbiting transition state/phase space theory (OTS/PST), were subsequently advanced by Klots[49−52] and highly developed by Chesnavich and Bowers.[53−56] In the latter OTS/PST, it is assumed that (1) an orbiting transition state is located at the reaction's centrifugal barrier and (2) that orbital rotational energy at this transition state is converted into relative translational energy of the products. For an isotropic long-range potential, OTS/PST is a variational unimolecular rate theory[11] which minimizes the reaction flux versus E, J, and orbital angular momentum, l.[30,57]

PST assumes the decomposition of a molecule or a collision complex is governed by the phase space available to each product under strict conservation of angular momentum and energy. The sum of states for the PST "transition state" is

$$N^{\ddagger}(E,J) = \int_0^{E-E_0} \rho_v^{\ddagger}(E - E_0 - E_{tr})\Gamma_{ro}^{\ddagger}(E_{tr},J)\, dE_{tr} \qquad (4)$$

where $\rho_v^{\ddagger}(E)$ is the vibrational density of states of the products at energy E, E_0 is the energy difference between reactants and products, $\Gamma_{ro}^{\ddagger}(E,J)$ is the sum of rotational-orbital states with rotational-orbital energy less than or equal to E, and E_{tr} is the sum of product translational and rotational energies. The product total energy is written as

$$E_\infty = E - E_0 = E_t + E_r + E_v = E_{tr} + E_v = E_t + E_{int} \qquad (5)$$

where E_∞ is the energy in excess of the classical threshold, E_v is the product vibrational energy, E_{int} is the product internal vibrational/rotational energy, E_t is the product relative translational energy, and E_r is the product rotational energy.

The differential total phase space volume accessible to the system,[53−56] as a function of product translational and rotational energy and product rotational and orbital quantum numbers j and l, is given by

$$\rho_v^{\ddagger}(E_\infty - E_t - E_r)\rho_r^{\ddagger}(E_r, j)\, dj\, dl\, dE_r\, dE_t \qquad (6)$$

In this equation, it is assumed for simplicity that the product pairs consist of one product with rotational quantum number j and an atom. In the formulation of PST for product pairs which do not include an atom, both product rotational quantum numbers have to be considered. The product rotational density of states $\rho_r^{\ddagger}(E_r, j)$ is given by

$$\rho_r^{\ddagger}(E_r,j) = \frac{\partial}{\partial E_r}\Gamma_r^{\ddagger}(E,J) \qquad (7)$$

where $\Gamma_r^{\ddagger}(E_r,J)$ is the sum of product rotational states with rotational energy equal or less than E_r and rotational angular momentum j. By combining eqs 4−7, one can write the rotational-orbital sum of states as[56]

$$\Gamma_{ro}^{\ddagger}(E_{tr},J) = \int\int \Gamma_r^{\ddagger}(E,J)\, dl\, dj \qquad (8)$$

This double integral has to be evaluated under strict conservation of total energy and angular momentum.

According to PST, the probability of forming products with given properties is proportional to the total phase space volume accessible to the system,[32−38] whose differential form is given by eq 6. The probability of forming products with translational and rotational energy E_{tr} is thus the integral of the aforementioned differential volume with fixed E_{tr}, and this leads to the following expression for the normalized kinetic energy release probability density

$$P_{E,J}(E_{tr}) = \frac{\rho_v^{\ddagger}(E - E_0 - E_{tr})\Gamma_{ro}^{\ddagger}(E_{tr},J)}{N^{\ddagger}(E,J)} \qquad (9)$$

Similarly, if one introduces the product rotational-orbital density of states as

$$\rho_{ro}^{\ddagger}(E_t,E_r,J) = \int\int \rho_r^{\ddagger}(E_r,j)\, dl\, dj \qquad (10)$$

the probability densities for translational and rotational energy are given respectively by

$$P_{E,J}(E_t) \alpha \int \rho_v^{\ddagger}(E - E_0 - E_{tr})\rho_{ro}^{\ddagger}(E_t,E_r,J)\, dE_r \qquad (11)$$

$$P_{E,J}(E_r) \alpha \int \rho_v^{\ddagger}(E - E_0 - E_{tr})\rho_{ro}^{\ddagger}(E_t,E_r,J)\, dE_t \qquad (12)$$

Similar expressions can be derived for rotational quantum number probability densities.

As described above, in PST the rotational-orbital sums and densities of state are evaluated at the product asymptotic limit. In contrast, for the OTS/PST model[53−56] they are evaluated at the orbiting transition state, which yields additional constraints on the values of the rotational and orbital quantum numbers in the above integral equations. This also has the effect of adding the height of the centrifugal barrier to E_t to obtain the product

TABLE 1: Classical Phase Space Theory (PST) and Orbiting Transition State/Phase Space Theory (OTS/PST) Predictions for $Al_6 \rightarrow Al_6 + Al$ Decomposition[a]

		symmetric top						spherical top					
		harmonic PST			anharmonic PST			anharmonic PST			anharmonic OTS/ PST		
E_∞	J[b]	$\langle E_{int}\rangle$[c]	$\langle j\rangle$[d]	j_{max}[e]	$\langle E_{int}\rangle$	$\langle j\rangle$	j_{max}	$\langle E_{int}\rangle$	$\langle j\rangle$	j_{max}	$\langle E_{int}\rangle$	$\langle j\rangle$	j_{max}
30.0	0	27.3	144	611	27.7	130	611	27.7	124	509	27.5	114	438
30.7	80	27.9	153	618	28.4	139	618	28.4	133	514	28.1	124	468
32.8	160	29.9	172	639	30.5	155	639	30.5	149	532	30.0	141	501
40.0	0	36.4	167	706	37.2	146	706	37.2	139	587	36.8	127	498
40.7	80	37.0	174	711	37.8	155	711	37.8	149	592	37.4	137	529
42.8	160	39.0	192	730	39.8	175	730	39.8	168	607	39.1	157	563
50.0	0	45.5	185	789	46.0	173	789	46.0	166	657	45.5	150	548
50.7	80	46.1	192	794	46.7	181	794	46.7	175	661	46.1	159	581
52.8	160	48.1	210	810	48.6	201	810	48.6	194	675	47.7	178	617
60.0	0	54.6	202	865	55.0	194	865	55.0	186	719	54.3	166	594
60.7	80	55.2	209	869	55.7	200	869	55.7	193	724	54.9	173	628
62.8	160	57.2	226	884	57.7	217	884	57.7	209	736	56.6	190	664
70.0	0	63.6	219	934	64.7	199	934	64.7	191	777	63.8	169	634
70.7	80	64.3	225	938	65.3	206	938	65.3	198	781	64.5	177	669
72.8	160	66.3	241	952	67.4	221	952	67.4	213	792	66.3	193	706
80.0	0	72.7	234	998	74.2	209	998	74.2	200	831	73.3	177	672
80.7	80	73.4	240	1002	74.9	215	1002	74.8	207	834	73.9	185	708
82.8	160	75.4	256	1015	76.8	232	1015	76.8	224	845	75.6	202	745

[a] Energies are in kcal/mol. [b] Total angular momentum quantum number. [c] Al_5 internal (rotational + vibrational) energy. [d] Al_5 rotational quantum number. [e] Al_5 maximum rotational quantum number.

TABLE 2: Classical Phase Space Theory (PST) and Orbiting Transition State/Phase Space Theory (OTS/PST) Predictions for $Al_{13} \rightarrow Al_{12} + Al$ Decomposition[a]

	symmetric top						spherical top					
	harmonic PST			anharmonic PST			anharmonic PST			anharmonic OTS/PST		
E_∞[b]	$\langle E_{int}\rangle$[c]	$\langle j\rangle$[d]	j_{max}[e]	$\langle E_{int}\rangle$	$\langle j\rangle$	j_{max}	$\langle E_{int}\rangle$	$\langle j\rangle$	j_{max}	$\langle E_{int}\rangle$	$\langle j\rangle$	j_{max}
85.0	82.3	317	2300	82.6	300	2300	82.6	268	1806	81.9	205	1072
110.0	106.6	360	2617	107.7	294	2617	107.7	262	2055	107.1	201	1182
135.0	130.8	399	2899	132.1	330	2899	132.1	295	2276	131.3	223	1276
160.0	155.0	434	3156	155.7	403	3156	155.7	362	2478	154.3	264	1359
185.0	179.2	467	3394	179.4	461	3394	179.4	414	2665	177.4	293	1434

[a] Energies are in kcal/mol. [b] Al_{13} vibrational energy in excess of the reaction threshold; $J = 0$. [c] Al_{12} internal (rotational + vibrational) energy. [d] Al_{12} rotational quantum number. [e] Al_{12} maximum rotational quantum number.

translational energy. For an isotropic long-range potential, $-C/r^n$, where $n = 4$ (ion-molecule interaction) or $n = 6$ (molecule-molecule interaction), there are analytic solutions for the OTS/PST rotational-orbital sums and densities of state.[53−56] The long-range isotropic interaction potentials, used for the OTS/PST calculations reported here, are of the form $-C/r^n$ and fit to the L-J/A-T potential of eqs 2 and 3. The fit is excellent and of the same quality as found previously,[1] for $Al_3 \rightarrow Al_2 + Al$; see Figure 30 of ref 1. The value of n is 6, and the parameter C is 1.4×10^5 kcal/mol Å^6 for $Al_6 \rightarrow Al_5 + Al$ and 5.4×10^5 kcal/mol Å^6 for $Al_{13} \rightarrow Al_{12} + Al$.

2. Comparison of PST and OTS/PST. Results of PST and OTS/PST calculations of the product average vibrational−rotational energy, $\langle E_{int}\rangle$; average rotational angular momentum, $\langle j\rangle$; and maximum j, (j_{max}), are given in Tables 1 and 2 for $Al_6 \rightarrow Al_5 + Al$ and $Al_{13} \rightarrow Al_{12} + Al$ decomposition, respectively. In these calculations, the effects of including anharmonicity in the product cluster's vibrational density of states[30] and treating the product cluster as a symmetric or spherical top are considered. The calculations also allow one to assess the differences in the PST and OTS/PST predictions of the product properties.

The symmetric and spherical top treatments of product cluster rotation give very similar results. The values of $\langle j\rangle$ and j_{max} are slightly smaller for the spherical top model, but the values of $\langle E_{int}\rangle$ are identical for the two models. As expected, including anharmonicity in the product's vibrational density of states increases $\langle E_{int}\rangle$, which will decrease $\langle E_t\rangle$ according to eq 5. OTS/PST calculates a statistical population of states at the centrifugal barrier, with the potential energy of this barrier transferred to product translation. As a result, OTS/PST gives smaller $\langle E_{int}\rangle$, $\langle j\rangle$, and j_{max} and higher $\langle E_t\rangle$ than does PST. In section IV, direct comparisons are made between the trajectory and anharmonic OTS/PST spherical top calculations.

B. Engelking Model. Engelking[5,6] has proposed a simplified version of phase space theory for relating the average product translational energy, $\langle E_t\rangle$, for dissociating a monomer from a cluster, i.e., $M_n \rightarrow M_{n-1} + M$, to the monomer's binding energy, E_0. The model is highly approximate in that angular momentum is not conserved and the density of states is approximated by the classical harmonic oscillator density. The model also assumes an equilibrium between the cluster M_n and its dissociation products $M_{n-1} + M$. With the above approximations, the unimolecular rate constant at energy E for forming products with translational energy E_t is

$$k(E,E_t) = 8\pi\sigma g\mu v^3(s-3)(s-2)(s-1)\frac{E_t(E-E_t)^{s-4}}{(E+E_0)^{s-1}} \quad (13)$$

where σ is the $M + M_{n-1} \rightarrow M_n$ association cross section, g is the reaction path degeneracy for M_n dissociation, μ is the $M_{n-1} + M$ reduced mass, v is the $M_{n-1} + M$ relative velocity, s is the number of vibrational degrees of freedom for M_n, and E_0 is

the monomer's binding energy. From eq 13, the probability of a particular E_t is

$$P_E(E_t)\,dE_t = \frac{k(E,E_t)\,dE_t}{\int_0^E k(E,E_t)\,dE_t} \quad (14)$$

The total rate constant is found by integrating over all the $k(E,E_t)$ to give

$$k(E) = \int_0^E k(E,E_t)\,dE_t = 8\pi\sigma g\mu v^3\,(s-1)\frac{E^{s-2}}{(E+E_0)^{s-1}} \quad (15)$$

The difference between this expression for $k(E)$ and the classical RRKM expression[11] $k(E) = \nu[E/(E+E_0)]^{s-1}$ is noteworthy. The average product translational energy determined from the distribution in eq 14 is

$$\langle E_t\rangle = \int_0^E E_t P_E(E_t)\,dE_t = \frac{2}{s-1} \quad (16)$$

Using this expression to replace E in eq 15 with $\langle E_t\rangle$ gives

$$E_0 = 0.5(s-1)[A^{1/(s-1)}\langle E_t\rangle^{(s-2)/(s-1)} - \langle E_t\rangle] \quad (17)$$

where $A = 16\ \pi\sigma g\mu\nu^3/k(E)$. This equation permits the determination of the monomer binding energy from the unimolecular rate constant $k(E)$, as defined by eq 15, and the experimental average product translational energy $\langle E_t\rangle$.

C. Klots Theory of Cluster Dissociation. Using ideas from thermal kinetics and the relationship between microcanonical and canonical ensembles, Klots[20−22] developed a theory for cluster dissociation based on thermodynamic properties. Excellent reviews of the theory are available,[11,58,59] and only the equations for relating $\langle E_t\rangle$ to the $M_n \rightarrow M_{n-1} + M$ dissociation energy are given here.

For a cluster dissociation with a loose transition state (i.e., no barrier for the reverse association reaction), it is argued that the average product translational energy is

$$\langle E_t\rangle = k_B T^{\ddagger} \quad (18)$$

where k_B is Boltzmann's constant and $T^{\ddagger}$ is the temperature of the transition state. More generally, Klots argues that $k_B T^{\ddagger} \le \langle E_t\rangle \le 2k_B T^{\ddagger}$,[60] where the lower bound of $\langle E_t\rangle$ is the phase space limit, eq 18, and is obtained when the orbital angular momentum barrier for the reverse association reaction is negligible, and the upper bound is a thermodynamic limit. It may be obtained from simple thermodynamic considerations by completely neglecting angular momentum conservation, which corresponds to cases where the orbital angular momentum barrier for the reverse association reaction is important. From similar arguments, the cluster heat capacity is given by

$$C_v = E_0/[k_B(T - T^{\ddagger})] \quad (19)$$

With the definition $T_b = (T + T^{\ddagger})/2$ and substituting $\langle E_t\rangle$ for $k_B T^{\ddagger}$ in eq 19, this equation may be rearranged to give

$$\langle E_t\rangle = \frac{E_0}{\gamma}\left\{1 - \frac{\gamma}{2C_v}\right\} \quad (20)$$

where $\gamma = E_0/k_B T_b$ is the Gspann parameter. A near constant value of 23.5 ± 1.5 has been suggested for γ for clusters metastable on the 10^{-5} s time scale.[11] The constancy of the Gspann parameter is closely related to Trouton's rule, which states that the entropy of vaporization $\Delta S_v = \Delta H_v/T_b$ is approximately constant.[11] With the value for the cluster heat capacity, eq 20 allows the determination of the $M_n \rightarrow M_{n-1} + M$ dissociation energy from the measured value of $\langle E_t\rangle$.

TABLE 3: Classical Trajectory Results for Al_6 Decomposition with Zero Total Angular Momentum[a]

	$Al_6 \rightarrow Al_5 + Al$ product energy partitioning[c]			
E_∞[b]	E_{int}[d]	E_v[e]	j[f]	j_{max}[g]
30.0	27.4 ± 0.1	25.6 ± 0.2	111 ± 3	273
40.0	36.4 ± 0.2	33.9 ± 0.2	133 ± 4	329
50.0	45.5 ± 0.2	42.4 ± 0.3	155 ± 4	484
60.0	54.4 ± 0.2	50.7 ± 0.3	172 ± 5	524
70.0	63.0 ± 0.3	58.9 ± 0.5	186 ± 5	560
80.0	71.9 ± 0.4	67.7 ± 0.5	196 ± 5	593

[a] Energies are in kcal/mol. The uncertainty in the trajectory value is the standard deviation of the mean. [b] Al_6 vibrational energy in excess of the reaction threshold. [c] $Al_6 \rightarrow Al_5 + Al$ product energy partitioning, obtained from the combined cluster trajectory ensembles initiated around the C_{2h}, C_{2v} and O_h minima. There are 100 reactive trajectories for each of these three ensembles. [d] Al_5 internal (rotational + vibrational) energy. [e] Al_5 vibrational energy. [f] Al_5 rotational quantum number. [g] Al_5 maximum rotational quantum number.

IV. Trajectory Results and Comparison with Statistical Theories

A. Al_6 Dissociation. Average trajectory values of the product energy and angular momentum for $Al_6 \rightarrow Al_5 + Al$ dissociation are listed in Table 3 for total angular momentum J of zero and in Table 4 for nonzero J. The results in Table 3 are an average of trajectories initialized around the C_{2h}, C_{2v} and O_h minima of Al_6, while those in Table 4 are for excitation about the O_h minimum. A comparison of the results in Table 3, with the $J = 0$ results in Table 4, shows the insensitivity of the product energy and angular momentum partitioning to which Al_6 minima is excited. The results in Table 4 show that, at the lower Al_6 energies, the Al_5 product angular momentum is somewhat dependent on the initial Al_6 angular momentum J. This dependency on J weakens as the Al_6 energy is increased.

Representative plots of the trajectory product energy and angular momentum distributions for Al_6 dissociation are illustrated in Figure 3. These are distributions of the product internal energy E_{int} and angular momentum j, for $E_\infty = 50$ kcal/mol and $J = 0$. As shown in these plots, the OTS/PST distributions are in excellent agreement with those determined from the trajectories. A more detailed comparison of the trajectory and OTS/PST product properties is given in Table 5, which shows overall excellent agreement between the trajectory and OTS/PST results. However, at the highest sets of E_∞ and J values the trajectory $\langle E_{int}\rangle$ and $\langle j\rangle$ are smaller and larger, respectively, than the OTS/PST values. Interestingly, a comparison of the trajectory j_{max} values in Tables 3 and 4 with the OTS/PST values in Table 1 shows that the actual dynamical (i.e. trajectory) value of j_{max} is smaller than the statistical (i.e., OTS/PST) prediction.

The above shows that OTS/PST is an excellent theoretical model for representing the product energy partitioning in $Al_6 \rightarrow Al_5 + Al$ dissociation. The agreement between the trajectory results and the predictions of the Engelking and Klots models for the product energy partitioning is less satisfactory. As shown in Figure 3, the Engelking model underestimates the high-energy component to the Al_5 internal energy distribution $P(E_{int})$ and, as a result, overestimates the average product translational energy $\langle E_t\rangle$_. This is shown in Table 6.

TABLE 4: Classical Trajectory Results for O_h Al_6 Decomposition with Non-zero Total Angular Momentum[a]

			$Al_6 \rightarrow Al_5 + Al$ product energy partitioning			
$E_{\infty,v}$[b]	f[c]	E_∞[d]	E_{int}[e]	E_v[f]	j[g]	j_{max}[h]
30.0	0	30.0	27.4 ± 0.2	25.7 ± 0.2	107 ± 6	273
30.0	40	30.2	27.6 ± 0.2	35.7 ± 0.3	113 ± 5	231
30.0	80	30.7	28.1 ± 0.2	26.0 ± 0.3	126 ± 5	285
30.0	120	31.6	28.7 ± 0.2	26.4 ± 0.3	132 ± 5	241
30.0	160	32.8	29.6 ± 0.2	26.9 ± 0.3	147 ± 6	303
40.0	0	40.0	36.5 ± 0.3	33.7 ± 0.4	142 ± 6	286
40.0	40	40.2	37.0 ± 0.3	34.8 ± 0.3	127 ± 6	298
40.0	80	40.7	37.4 ± 0.3	34.5 ± 0.3	149 ± 6	313
40.0	120	41.6	38.1 ± 0.3	35.3 ± 0.4	150 ± 6	324
40.0	160	42.9	38.8 ± 0.3	35.7 ± 0.4	155 ± 6	326
50.0	0	50.0	45.8 ± 0.3	42.8 ± 0.4	150 ± 8	373
50.0	40	50.2	46.0 ± 0.3	43.2 ± 0.4	143 ± 7	372
50.0	80	50.7	46.8 ± 0.3	44.2 ± 0.4	144 ± 8	459
50.0	120	51.6	46.6 ± 0.3	43.4 ± 0.4	160 ± 7	398
50.0	160	52.9	47.6 ± 0.4	43.5 ± 0.5	186 ± 8	379
60.0	0	60.0	54.5 ± 0.4	50.5 ± 0.5	174 ± 8	451
60.0	40	60.2	55.2 ± 0.4	52.0 ± 0.5	154 ± 8	375
60.0	80	60.7	54.6 ± 0.4	50.5 ± 0.5	185 ± 9	433
60.0	120	61.6	56.7 ± 0.4	52.4 ± 0.6	198 ± 7	377
60.0	160	62.8	56.9 ± 0.4	52.8 ± 0.6	185 ± 8	440
70.0	0	70.0	63.9 ± 0.5	60.0 ± 0.7	190 ± 9	440
70.0	40	70.2	63.4 ± 0.5	58.7 ± 0.7	201 ± 9	464
70.0	80	70.7	63.9 ± 0.5	59.6 ± 0.7	191 ± 8	385
70.0	120	71.6	64.3 ± 0.5	59.0 ± 0.6	225 ± 8	426
70.0	160	72.8	65.2 ± 0.5	60.5 ± 0.6	202 ± 8	438
80.0	0	80.0	71.8 ± 0.6	67.7 ± 0.7	193 ± 9	439
80.0	40	80.2	71.8 ± 0.6	66.8 ± 0.8	210 ± 9	434
80.0	80	80.7	73.1 ± 0.6	68.0 ± 0.8	218 ± 9	413
80.0	120	81.6	72.4 ± 0.7	67.7 ± 0.8	225 ± 9	526
80.0	160	82.8	73.5 ± 0.7	68.5 ± 0.8	231 ± 9	538

[a] Energies are in kcal/mol. Each ensemble contains 100 reactive trajectories. The uncertainty in the trajectory value is the standard deviation of the mean. [b] Al_6 initial vibrational energy in excess of the reaction threshold. [c] Al_6 total angular momentum quantum number. [d] Al_6 initial total or internal (vibrational + rotational) energy in excess of the reaction threshold. [e] Al_5 internal (rotational + vibrational) energy. [f] Al_5 vibrational energy. [g] Al_5 rotational quantum number. [h] Al_5 maximum rotational quantum number.

The Klots value for $\langle E_t \rangle$, calculated from eq 20 using the actual threshold E_0 of 43.8 kcal/mol, a reduced heat capacity C_v of 12, and the usual 23.5 Gspann parameter γ, is much too small and equals 0.04 kcal/mol. This suggests that the Klots model together with the usual 23.5 Gspann parameter, which has been advanced for clusters metastable on the 10^{-5} s time scale, cannot be applied to clusters with lifetimes on the nanosecond time scale, such as the Al_n clusters investigated here.[30] Consequently, no attempt was made in this work to use this Klots model to extract binding energies from the Al_n product energy distributions.

Another approach advanced by Klots[61,62] involves calculating a temperature for the products (i.e. loose transition state) from the expression

$$E_\infty = \frac{r-1}{2} k_B T^\ddagger + k_B T^\ddagger + skT^\ddagger \qquad (21)$$

where r and s are the number of rotational and vibrational degrees of freedom, respectively. (The vibrations are treated classically for this classical simulation. In using this model to compare with experiment, the quantum mechanical expression is used for the vibrational thermal energy.[61,62]) When $T^\ddagger$ calculated from eq 21 is inserted into eq 18 to find $\langle E_t \rangle$, approximate agreement is found with the trajectory results, as shown in Table 6. As argued by Klots,[60] $\langle E_t \rangle$ is bound by $k_B T^\ddagger$ (i.e., eq 18) and $2k_B T^\ddagger$, but it is closer to the phase space limit of $k_B T^\ddagger$. Conversely, the prediction of the Engelking model lies

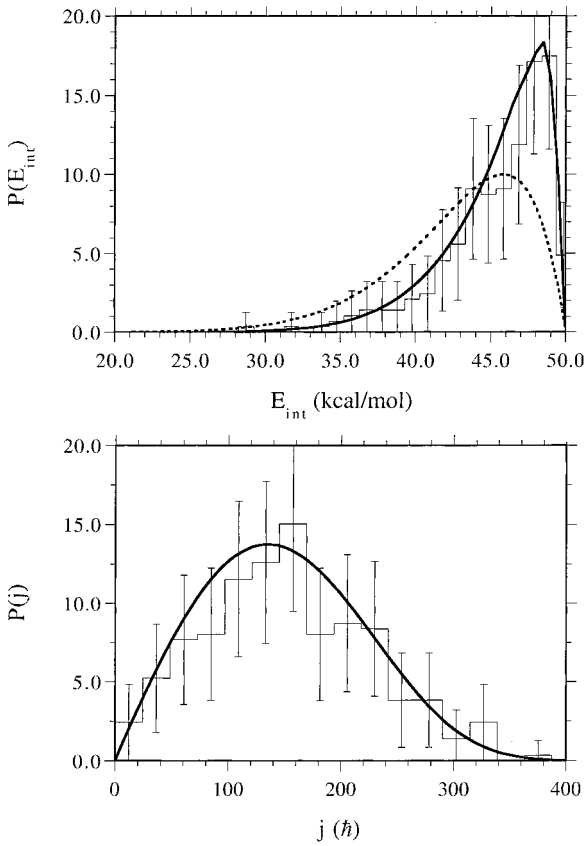

Figure 3. Product internal energy (E_{int}) and angular momentum (j) distributions for $Al_6 \rightarrow Al_5 + Al$ unimolecular fragmentation, E_∞ = 50 kcal/mol and $J = 0$. The histograms are distributions obtained from trajectory calculations. The solid thick lines represent the OTS/PST predictions and the dash lines those of the Engelking model.

TABLE 5: Comparison of Trajectory and OTS/PST Values of Average Product Properties for $Al_6 \rightarrow Al_5 + Al$ Dissociation[a]

			$\langle E_{int} \rangle$[e]		$\langle j \rangle$[f]	
$E_{\infty,v}$[b]	J[c]	E_∞[d]	trajectory	OTS/PST[g]	trajectory	OTS/PST
30.0	0	30.0	27.4 ± 0.2	27.5	107 ± 6	114
30.0	80	30.7	28.1 ± 0.2	28.1	126 ± 5	124
30.0	160	32.8	29.6 ± 0.2	30.0	147 ± 6	141
40.0	0	40.0	36.5 ± 0.3	36.8	142 ± 6	127
40.0	80	40.7	37.4 ± 0.3	37.4	149 ± 6	137
40.0	160	42.9	38.8 ± 0.3	39.1	155 ± 6	157
50.0	0	50.0	45.8 ± 0.3	45.5	150 ± 8	150
50.0	80	50.7	46.8 ± 0.3	46.1	144 ± 8	159
50.0	160	52.9	47.6 ± 0.4	47.7	186 ± 8	178
60.0	0	60.0	54.5 ± 0.4	54.3	174 ± 8	166
60.0	80	60.7	54.6 ± 0.4	54.9	185 ± 9	173
60.0	160	62.8	56.9 ± 0.4	56.6	185 ± 8	190
70.0	0	70.0	63.9 ± 0.5	63.8	190 ± 9	169
70.0	80	70.7	63.9 ± 0.5	64.5	191 ± 8	177
70.0	160	72.8	65.2 ± 0.5	66.3	202 ± 8	193
80.0	0	80.0	71.8 ± 0.6	73.3	193 ± 9	177
80.0	80	80.7	73.1 ± 0.6	73.9	218 ± 9	185
80.0	160	82.8	73.5 ± 0.7	75.6	231 ± 9	202

[a] Energies are in kcal/mol. The uncertainty in the trajectory value is the standard deviation of the mean. [b] Al_6 initial vibrational energy in excess of the reaction threshold. [c] Al_6 total angular momentum quantum number. [d] Al_6 initial total or internal (vibrational + rotational) energy in excess of the reaction threshold. [e] Al_5 internal (rotational + vibrational) energy. [f] Al_5 rotational quantum number. [g] The OTS/PST values are those for the anharmonic OTS/PST spherical top calculation in Table 1.

TABLE 6: Comparison of Trajectory Results and Statistical Models for Describing $Al_n \rightarrow Al_{n-1} + Al$ Dissociation[a]

		$\langle E_t \rangle$					predicted E_0
$E_{\infty,v}$[b]	J[c]	E_∞[d]	trajectory[e]	OTS/PST	Engelking[f]	Klots[g]	Engelking[h]
				$Al_6 \rightarrow Al_5 + Al$			
30.0	0	30.0	2.6	2.5	5.5	2.1	2.0
30.0	160	32.8	3.2	2.8	6.0	2.3	2.2
40.0	0	40.0	3.5	3.4	7.3	2.9	2.7
40.0	160	42.9	4.1	3.8	7.8	3.1	2.9
50.0	0	50.0	4.2	4.5	9.1	3.6	3.5
50.0	160	52.9	5.3	5.2	9.6	3.8	3.8
60.0	0	60.0	5.5	5.7	10.9	4.3	4.3
60.0	160	62.8	5.9	6.2	11.4	4.5	4.6
70.0	0	70.0	6.1	6.2	12.7	5.0	4.8
70.0	160	72.8	7.6	6.5	13.2	5.2	5.0
80.0	0	80.0	8.2	6.7	14.5	5.7	5.3
80.0	160	82.8	9.3	7.2	15.1	5.9	5.6
				$Al_{13} \rightarrow Al_{12} + Al$			
110.0	0	110.0	4.1	2.9	6.9	3.1	2.2
135.0	0	135.0	4.3	3.7	8.4	3.9	2.8
160.0	0	160.0	5.5	5.7	10.0	4.6	3.8
185.0	0	185.0	6.8	7.6	11.6	5.3	4.8

[a] Energies are in kcal/mol. [b] Al_n initial vibrational energy in excess of the reaction threshold. [c] Al_n total angular momentum quantum number. [d] Al_n initial total or internal (vibrational + rotational) energy in excess of the reaction threshold. [e] The uncertainty in the trajectory value is given in Table 2; i.e., $E_\infty = \langle E_{int} \rangle + \langle E_t \rangle$ [f] Calculated from eq 16. [g] Calculated from eqs 18 and 21. [h] Calculated from eq 17 using the OTS/PST value for $\langle E_t \rangle$.

TABLE 7: Classical Trajectory Results of Al_{13} Decomposition with Zero Total Angular Momentum[a]

	$Al_{13} \rightarrow Al_{12} + Al$ product energy partitioning			
E_∞[b]	E_{int}[c]	E_v[d]	j[e]	j_{max}[f]
110.0	105.9 ± 0.4	105.2 ± 0.5	237 ± 17	546
135.0	130.7 ± 0.2	129.9 ± 0.2	239 ± 8	1225
160.0	154.5 ± 0.3	153.6 ± 0.3	277 ± 10	1481
185.0	178.2 ± 0.3	177.1 ± 0.4	331 ± 14	2361

[a] Energies are in kcal/mol. Ensembles contain 200 reactive trajectories, 100 sampled around both the D_{2h} and D_{3d} (fcc) minima (except for $E_\infty = 110.0$ kcal, where the ensemble only contains 50 reactive trajectories). The uncertainty is the standard deviation of the mean. [b] Vibrational energy of Al_{13} in excess of the dissociation threshold. [c] Al_{12} internal (rotational + vibrational) energy. [d] Al_{12} rotational quantum number. [e] Al_{12} rotational quantum number. [f] Al_{12} maximum rotational quantum number.

closely to the thermodynamic limit of $2k_BT^{\ddagger}$, which is not too surprising, since the Engelking model was derived employing thermodynamic considerations.

Using eq 17, the Engelking model provides a means to predict the $M_n \rightarrow M_{n-1} + M$ dissociation energy from an experimental measurements of $\langle E_t \rangle$. The calculations performed here provide a means to study this equation. The trajectory calculations indicate that OTS/PST predicts accurate product properties and, thus, OTS/PST may be used to determined $\langle E_t \rangle$ for $Al_6 \rightarrow Al_5 + Al$ dissociation. This value may then be inserted into eq 17 to determine the E_0 values predicted by the Engelking model, which may be compared with the actual E_0 of 43.8 kcal/mol. In solving eq 17 for the Engelking model, eq 15 was used for $k(E)$. The results of this analysis are given in Table 6, where it is seen that the Engelking E_0 values are too small by an order of magnitude. In comparison to the utility of the Engelking model for fitting experimental data,[11] when the equations of this model are used in an exact and consistent manner, as is done here, they are found to give highly inaccurate E_0 values.

B. Al_{13} Dissociation. Average trajectory values of the product energy and angular momentum values for $Al_{13} \rightarrow Al_{12} + Al$ dissociation, with zero total angular momentum, are listed in Table 7. The Al_{12} product rotational angular momentum is only weakly dependent on the total energy and similar to what is found for the Al_5 product in Table 3. The form of the product internal energy E_{int} and angular momentum j distributions for $Al_{13} \rightarrow Al_{12} + Al$ are illustrated in Figure 4 for an excess energy of 185 kcal/mol and zero angular momentum.

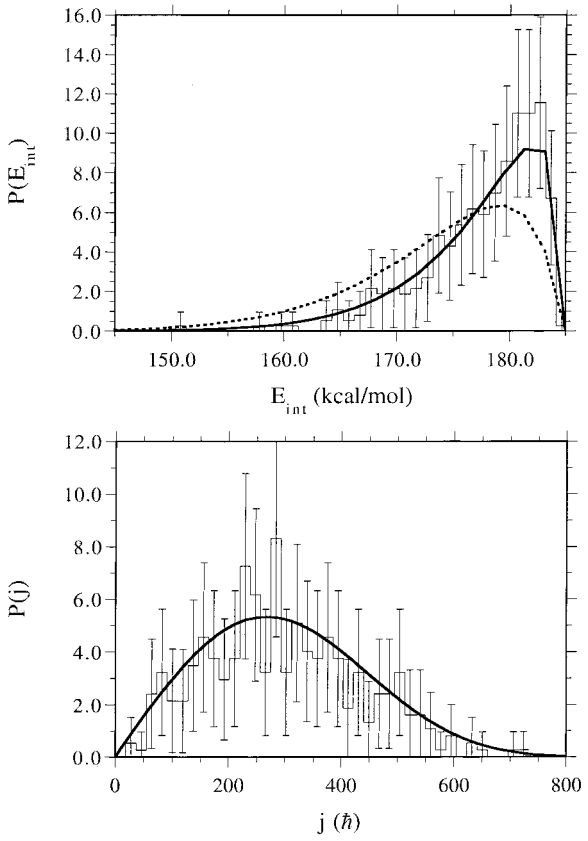

Figure 4. Product internal energy (E_{int}) and angular momentum (j) distributions for $Al_{13} \rightarrow Al_{12} + Al$ unimolecular fragmentation, $E_\infty = 185$ kcal/mol and $J = 0$. The histograms are distributions obtained from trajectory calculations. The solid thick lines represent the OTS/PST predictions and the dash lines those of the Engelking model.

Figure 4 shows that the OTS/PST distributions of E_{int} and j are in excellent agreement with the trajectory results. The

TABLE 8: Comparison of Trajectory and OTS/PST values of Average Product Properties for $Al_{13} \rightarrow Al_{12} + Al$ Dissociation[a]

	$\langle E_{int}\rangle$[c]		$\langle j\rangle$[d]		j_{max}[e]	
E_∞[b]	trajectory	OTS/PST[f]	trajectory	OTS/PST	trajectory	OTS/PST
110	105.9 ± 0.4	107.0	237 ± 17	201	546	1182
135	130.7 ± 0.2	131.3	239 ± 8	223	1225	1276
160	154.5 ± 0.3	154.3	277 ± 10	264	1481	1359
185	178.2 ± 0.3	177.4	331 ± 14	293	2361	1434

[a] Energies are in kcal/mol. The uncertainty in the trajectory values is the standard deviation of the mean. [b] The Al_{13} total momentum is zero. E_∞ is the Al_{13} initial vibrational energy in excess of the dissociation threshold. [c] Al_{12} internal (rotational + vibrational) energy. [d] Al_{12} rotational quantum number. [e] Al_{12} maximum rotational quantum number. [f] The OTS/PST values are those for the anharmonic OTS/PST spherical top calculations in Table 2.

comparison of trajectory and OTS/PST values of $\langle E_{int}\rangle$, $\langle j\rangle$, and j_{max} in Table 8, for all the E_∞ considered, shows that there is overall good agreement between the trajectory and OTS/PST product properties for $Al_{13} \rightarrow Al_{12} + Al$ dissociation. The largest difference between the two $\langle E_{int}\rangle$ values is at the lowest E_∞ of 110 kcal/mol.

As found above for Al_6 decomposition, when used in an exact, consistent manner, the Engelking model does not give accurate product energy partitioning for Al_{13} decomposition. This is shown in Figure 4 and Table 6. The Engelking model underestimates the high energy part of the Al_{12} internal energy distribution and therefore predicts $\langle E_t\rangle$ values that are too large. The Klots model, as represented by eq 20 and applied as described above for Al_6 decomposition, gives a value for $\langle E_t\rangle$ of 1.54 kcal/mol, which is again too small, possibly because the Gspann parameter of 23.5 used in the Klots model is not appropriate for clusters with lifetimes shorter than 10^{-5} s. However, as found for Al_6 decomposition, using eq 21 to calculate a product temperature and then using eq 18 to determine $\langle E_t\rangle$ is a model that gives an $\langle E_t\rangle$ in approximate agreement with the trajectory results. This is shown in Table 6. As observed for Al_6 decomposition, the trajectory $\langle E_t\rangle$ is bound by $k_BT^\ddagger$ (i.e., eq 18) and $2k_BT^\ddagger$, but it is much closer to the phase space limit of $k_BT^\ddagger$. The predictions of the Engelking model are again closer to the thermodynamic limit of $2k_BT^\ddagger$. The comparison, in Table 6, of the dissociation threshold E_0 predicted by the Engelking model, with the actual value of 56.2 kcal/mol, shows that the Engelking threshold is a factor of 5−10 too small.

V. Summary

From the work presented here, the following conclusions may be made concerning the classical trajectory product energy and angular momentum distributions for $Al_6 \rightarrow Al_5 + Al$ and $Al_{13} \rightarrow Al_{12} + Al$ dissociation and the ability of statistical theories to accurately model these trajectory results.

PST, which assumes a statistical population of states at the product asymptotic limit, gives larger product rotational and vibrational energies than does OTS/PST, which assumes this statistical population exists at the centrifugal barrier. OTS/PST gives a larger value for the average product relative translational energy $\langle E_t\rangle$.

Including anharmonicity in the product vibrational density of states decreases the average product relative translational energy $\langle E_t\rangle$ predicted by both PST and OTS/PST.

Given the statistical uncertainties, the product energy and angular momentum partitioning predicted by OTS/PST is in overall excellent agreement with the trajectory results.

When used in an exact, consistent way, the Engelking statistical model predicts product energy partitioning for Al_6 and Al_{13} dissociation much different than the trajectory results. One Klots model yields very inaccurate energy partitioning for Al_6 and Al_{13} dissociation, which suggests that the model is not applicable to clusters with lifetimes shorter than the 10^{-5} s time scale. However, another less approximate Klots model, more closely tied to PST, gives more accurate $\langle E_t\rangle$ values. The model proposed by Engelking for deducing the cluster dissociation energy E_0 from a measurement of $\langle E_t\rangle$ does not give accurate results for Al_6 and Al_{13} dissociation. In contrast to these findings, previous work[11,58,59] has shown that the Engelking and Klots models are very useful for fitting experimental results.

Acknowledgment. The authors wish to thank Tomas Baer and Cornelius Klots for very valuable discussions concerning cluster dissociation. This research was funded by the Natural Sciences and Engineering Research Council of Canada (G.H.P.) and the National Science Foundation (W.L.H.).

References and Notes

(1) *Chemical Reactions in Clusters*; Bernstein, E. R., Ed.; Oxford: New York, 1996.
(2) Castleman, A. W.; Bowen, K. H. *J. Phys. Chem.* **1996**, *100*, 12911.
(3) Bréchignac, C.; Cahuzac, P.; Leygnier, J.; Weiner, J. *J. Chem. Phys.* **1989**, *90*, 1492.
(4) Bréchignac, C.; Cahuzac, P.; Leygnier, J.; Pflaum, R.; Roux, J. P.; Weiner, J. *Zeitschrift Phys. D* **1989**, *12*, 199.
(5) Engelking, P. C. *J. Chem. Phys.* **1986**, *85*, 3103.
(6) Engelking, P. C. *J. Chem. Phys.* **1987**, *87*, 936.
(7) Wei, S.; Tzeng, W. B., Jr.; Castleman, A. W. *J. Chem. Phys.* **1990**, *92*, 332.
(8) Wei, S.; Tzeng, W. B., Jr.; Castleman, A. W. *J. Chem. Phys.* **1990**, *93*, 2506.
(9) Wei, S.; Kilgore, K.; Tzeng, W. B., Jr.; Castleman, A. W. *J. Phys. Chem.* **1991**, *95*, 8306.
(10) Shi, Z.; Ford, V.; Wei, S., Jr.; Castleman, A. W. *J. Chem. Phys.* **1993**, *99*, 8009.
(11) Baer, T.; Hase, W. L. *Unimolecular Reaction Dynamics*; Oxford: New York, 1996.
(12) Rodgers, M. T.; Ervin, K. M.; Armentrout, P. B. *J. Chem. Phys.* **1997**, *106*, 4499.
(13) Rodgers, M. T.; Armentrout, P. B. *J. Chem. Phys.* **1998**, *109*, 1787.
(14) Spasov, V. A.; Ervin, K. M. *J. Chem. Phys.* **1998**, *109*, 5344.
(15) Ray, U.; Jarrold, M. F.; Bower, J. E.; Kraus, J. S. *J. Chem. Phys.* **1989**, *91*, 2912.
(16) Jarrold, M. F.; Creegan, K. M. *Int. J. Mass Spectrom. Ion Processes* **1990**, *102*, 161.
(17) Ingolfsson, O.; Takeo, H.; Nonose, S. *J. Chem. Phys.* **1999**, *110*, 4382.
(18) Ingolfsson, O.; Busolt, U.; Sugawara, K. *J. Chem. Phys.* **2000**, *112*, 4613.
(19) Rao, B. K.; Jena, P. *J. Chem. Phys.* **1999**, *111*, 1890.
(20) Klots, C. E. *J. Phys. Chem.* **1988**, *92*, 5864.
(21) Klots, C. E. *J. Chem. Phys.* **1989**, *90*, 4470.
(22) Klots, C. E. *J. Phys. Chem.* **1992**, *96*, 1733.
(23) Tzeng, W. B.; Wei, S.; Castleman, A. W. *J. Phys. Chem.* **1991**, *95*, 5757.
(24) Weerasinghe, S.; Amar, F. G. *J. Chem. Phys.* **1993**, *98*, 4967.
(25) Lifshitz, C.; Louage, F. *Int. J. Mass Spectrom. Ion Proc.* **1990**, *101*, 202.
(26) Sato, H.; Matsuzaki, A.; Nishio, S.; Ito, O.; Furukawa, K.; Kawasaki, T. *J. Chem. Phys.* **1998**, *108*, 3940.
(27) Atrill, S.; Stace, A. J. *J. Chem. Phys.* **1998**, *108*, 1924.
(28) Peslherbe, G. H.; Hase W. L. *J. Chem. Phys.* **1994**, *101*, 8535.
(29) Peslherbe, G. H.; Hase, W. L. *J. Chem. Phys.* **1996**, *104*, 9445.
(30) Peslherbe, G. H.; Hase, W. L. *J. Chem. Phys.* **1996**, *105*, 7432.
(31) Bunker, D. L.; Hase, W. L. *J. Chem. Phys.* **1973**, *59*, 4621.
(32) Light, J. C. *J. Chem. Phys.* **1964**, *40*, 3221.
(33) Pechukas, P.; Light, J. C. *J. Chem. Phys.* **1965**, *42*, 3281.
(34) Light, J. C.; Lin, J. *J. Chem. Phys.* **1965**, *43*, 3209.
(35) Nikitin, E. *Theor. Exp. Chem.* **1965**, *1*, 83.
(36) Pechukas, P.; Light, J. C.; Rankin, C. *J. Chem. Phys.* **1966**, *44*, 794.
(37) Lin, J.; Light, J. C. *J. Chem. Phys.* **1966**, *45*, 2545.
(38) Light, J. C. *Discuss. Faraday Soc.* **1967**, *44*, 14.

(39) Peslherbe, G. H.; Hase, W. L. In *Theory of Atomic and Molecular Clusters*; Jellinek, J., Ed.; Springer: New York, 1999; pp 228−254.
(40) Hase, W. L.; Duchovic, R. J.; Hu, X.; Komornicki, A.; Lim, K. F.; Lu, D.-H.; Peslherbe, G. H.; Swamy, K. N.; Vande Linde, S. R.; Varandas, A.; Wang, H.; Wolf, R. J. *QCPE* **1996**, *16*, 671.
(41) Pettersson, L. G. M.; Bauschlicher, C. W.; Halicioglu, T. *J. Chem. Phys*. **1987**, *87*, 2205.
(42) Johnston, R. L.; Fang, J. Y. *J. Chem. Phys.* **1992**, *97*, 7809.
(43) Erkoc, S. *Phys. Status Solidi B* **1989**, *152*, 447.
(44) Erkoc, S. *Phys. Status Solidi B* **1990**, *161*, 211.
(45) Erkoc, S. *Z. Phys. D* **1991**, *19*, 423.
(46) El-Bayyari, Z.; Erkoc, S. *Phys. Status Solidi B* **1992**, *170*, 103.
(47) Hase, W. L.; Buckowski, D. *Chem. Phys. Lett.* **1980**, *74*, 284.
(48) Bolton, K.; Hase, W. L.; Peslherbe, G. H. In *Modern Methods for Multidimensional Dynamics Computations in Chemistry*; Thompson, D. L., Ed.; World Scientific: River Edge, NJ, 1998; pp 143−189.
(49) Klots, C. E. *J. Phys. Chem.* **1971**, *75*, 1526.
(50) Klots, C. E. *Z. Naturforsch., Teil A* **1972**, *27*, 553.
(51) Klots, C. E. *J. Chem. Phys.* **1976**, *64*, 4269.
(52) Klots, C. E.; Mintz, D.; Baer, T. *J. Chem. Phys.* **1977**, *66*, 5100.
(53) Chesnavich, W. J.; Bowers, M. T. *J. Am. Chem. Soc.* **1976**, *98*, 8301.
(54) Chesnavich, W. J.; Bowers, M. T. *J. Am. Chem. Soc.* **1977**, *99*, 1705.
(55) Chesnavich, W. J.; Bowers, M. T. *J. Chem. Phys.* **1977**, *66*, 2306.
(56) Chesnavich, W. J.; Bowers, M. T. In *Gas-Phase Ion Chemistry*; Bowers, M. T., Ed.; Academic Press: New York, 1979.
(57) Chesnavich, W. J.; Bowers, M. T. *Prog. React. Kinet.* **1982**, *11*, 137.
(58) Klots, C. E. In *Cluster Ions*; Baer, T., Ng, C. Y., Powis, I., Eds.; Wiley: New York, 1994.
(59) Lifshitz, C. In *Cluster Ions*; Baer, T., Ng, C. Y., Powis, I., Eds; Wiley: New York, 1993.
(60) Klots, C. E. *J. Chem. Phys.* **1993**, *98*, 1110.
(61) Klots, C. E. *J. Chem. Phys.* **1973**, *58*, 5364.
(62) See eq 9.18 in ref 11 and neighboring discussion.